Journal of Hazardous Materials 518 (2026) 143996

Contents lists available at ScienceDirect

Journal of Hazardous Materials

journal homepage: www.elsevier.com/locate/jhazmat

Component-specific effects shape shifts between synergism and antagonism in organophosphate ester mixtures

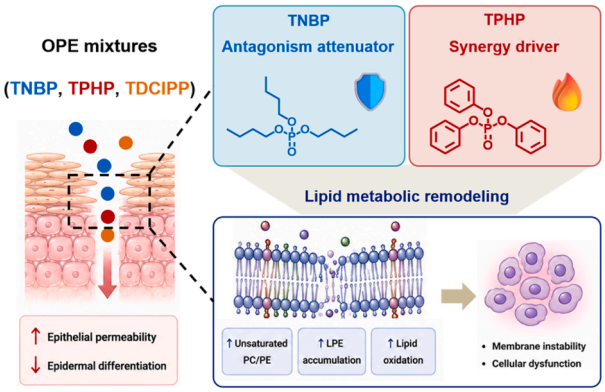
Na Luo [a,b], Guiying Li [a,b], Yanpeng Gao [a,b], Taicheng An [a,b,*]

[a] Guangdong-Hong Kong-Macao Joint Laboratory for Contaminants Exposure and Health, Guangdong Key Laboratory of Environmental Catalysis and Health Risk Control, Institute of Environmental Health and Pollution Control, Guangdong University of Technology, Guangzhou, China
[b] Guangdong Basic Research Center of Excellence for Ecological Security and Green Development, Guangzhou Key Laboratory of Environmental Catalysis and Pollution Control, School of Environmental Science and Engineering, Guangdong University of Technology, Guangzhou, China

HIGHLIGHTS

- OPE mixtures show dynamic shifts between synergism and antagonism to HaCaT cells.
- TPHP drives synergistic toxicity, while TNBP attenuates OPE mixture effects.
- OPE mixtures disrupt epithelial permeability and stratum corneum differentiation.
- Lipid remodeling links membrane instability to dermal OPE mixture toxicity.

GRAPHICAL ABSTRACT



ARTICLE INFO

Keywords:
Organophosphate esters
Mixture toxicity
Dermal exposure
Lipid metabolism
Non-additive effects

ABSTRACT

Organophosphate esters (OPEs) frequently co-occur in human exposure, yet their combined hazards cannot be reliably inferred from single-compound toxicity. How individual OPEs reshape non-additive effects across compositions and effect levels remains unclear. Here, we investigated interaction patterns and associated biological responses of representative OPE mixtures, including tributyl phosphate (TNBP), triphenyl phosphate (TPHP), and tris(1,3-dichloro-2-propyl) phosphate (TDCIPP), using human keratinocytes as a dermal exposure model. Combination index (CI) analysis revealed composition- and effect-level-dependent interactions. Ternary mixtures exhibited distinct composition-dependent CI–Fa trajectories, with some compositions trending toward additivity at higher effect levels, whereas TPHP-rich mixtures showed progressively stronger synergism. Binary mixtures showed pair-dependent interactions, with TPHP–TDCIPP and TNBP–TDCIPP exhibiting contrasting interaction modes. At total nominal molar concentrations of 0.1, 1, and 10 μM for the 1:1:1 ternary mixture, co-exposure modestly increased HaCaT monolayer permeability, reaching statistical significance at 10 μM, and altered differentiation-related gene expression, revealing barrier-associated effects. Untargeted metabolomics of individual and mixture exposures further revealed distinct lipid remodeling patterns, including interaction-

* Corresponding author at: Guangdong-Hong Kong-Macao Joint Laboratory for Contaminants Exposure and Health, Guangdong Key Laboratory of Environmental Catalysis and Health Risk Control, Institute of Environmental Health and Pollution Control, Guangdong University of Technology, Guangzhou, China.
E-mail address: antc99@gdut.edu.cn (T. An).

https://doi.org/10.1016/j.jhazmat.2026.143996
Received 11 August 2026; Received in revised form 19 October 2026; Accepted 21 October 2026
Available online 22 October 2026
0304-3894/© 2026 Elsevier B.V. All rights are reserved, including those for text and data mining, AI training, and similar technologies.

associated differences in glycerophospholipid responses. Collectively, OPE mixture hazards depend not only on individual toxicity but also on the capacity of specific components to modify combined effects, supporting improved mixture hazard characterization and prioritization of interaction-modifying contaminants.

1. Introduction

Chemical risk assessment has traditionally been established on the basis of individual chemicals, assuming that toxicity can be evaluated according to compound-specific properties and exposure levels [1–3]. However, humans are rarely exposed to isolated chemicals in real-world environments but instead encounter complex mixtures originating from consumer products, industrial activities, and environmental contamination [4–6]. Increasing evidence indicates that interactions among chemical components can generate synergistic, additive, or antagonistic effects, resulting in mixture toxicity that cannot be accurately predicted from single-chemical responses [7–9]. This discrepancy introduces substantial uncertainty into current health risk assessment. Previous studies have applied the Chou–Talalay method to quantify mixture interactions across effect levels, which may provide a useful framework for characterizing effect-level-dependent interaction profiles [10]. Although mixture toxicity has been increasingly recognized as an important challenge, the biological basis underlying differences in mixture interaction profiles across effect levels remains insufficiently characterized.

Organophosphate esters (OPEs) provide an environmentally relevant model for investigating the mechanisms underlying chemical mixture toxicity [11]. Following the phase-out of brominated flame retardants, OPEs have been widely used as alternative flame retardants and plasticizers, leading to their widespread occurrence in indoor environments and human exposure-related matrices [12–15]. Unlike chemicals evaluated individually under conventional risk assessment frameworks, OPEs commonly occur as complex mixtures containing structurally diverse compounds, including alkyl-, aryl-, and chlorinated OPEs. Among them, tributyl phosphate (TNBP), triphenyl phosphate (TPHP), and tris(1,3-dichloro-2-propyl) phosphate (TDCIPP) are frequently detected together in human samples and exhibit distinct physicochemical properties and biological activities [16–18]. For example, TNBP, TPHP, and TDCIPP were detected in human serum at detection frequencies of 83%, 76%, and 59%, respectively, with mean concentrations of 3.63, 2.03, and 0.09 μg/L [19]. Previous studies have demonstrated that individual OPEs can induce oxidative stress, endocrine disruption, metabolic disturbance, and developmental toxicity [20]. However, whether different OPE components contribute equally to mixture toxicity, or whether specific components exert distinct regulatory roles within mixtures, remains unclear.

Human exposure to OPEs occurs through multiple pathways, including inhalation, ingestion, and dermal contact [21]. Although ingestion is usually considered the primary exposure route for the general population, increasing evidence highlights dermal contact as another important pathway [22]. For instance, several studies have demonstrated that dermal exposure to OPEs exceeds inhalation exposure in children [23]. Dermal contact with OPEs via dust, soil, and water has resulted in an estimated daily intake of 3.54 ng/kg BW/d, significantly surpassing that from diet (0.18 ng/kg BW/d) [24]. Besides, dermal exposure represents an important but insufficiently characterized pathway for human exposure to OPE mixture because the skin serves not only as a direct contact surface but also as a dynamic biological barrier regulating chemical penetration and internal susceptibility [25]. The integrity of the epidermal barrier depends on coordinated cellular differentiation and lipid homeostasis, with ceramides, cholesterol, and free fatty acids constituting the major lipid components of the stratum corneum [26]. Glycerolipid and glycerophospholipid metabolism may additionally influence keratinocyte membrane organization and cellular signaling, thereby modifying cellular responses to environmental chemicals [27]. Therefore, lipid metabolic remodeling may provide a mechanistic link between chemical mixture exposure, differential biological responses, and mixture toxicity outcomes. The Chou–Talalay method can characterize mixture interaction profiles across effect levels, providing a basis for exploring their potential biological determinants [10]. However, the contribution of component-specific lipid responses to these effect-level-dependent interaction patterns remains insufficiently understood.

Here, we selected three representative OPEs (TNBP, TPHP, and TDCIPP) to investigate how chemical mixtures generate variable toxicity responses and to identify potential biological mechanisms underlying these interactions using human keratinocytes as a dermal exposure model. By integrating combination index analysis, barrier function assessment, and untargeted metabolomics, this study aimed to (i) characterize the dynamic interaction patterns of OPE mixtures across different compositions and effect levels; (ii) identify the distinct roles of individual components in shaping mixture toxicity; and (iii) elucidate lipid metabolic alterations associated with component-specific toxicity responses. These findings provide new insights into the mechanisms underlying complex chemical mixture toxicity and contribute to the development of mechanism-informed approaches for environmental health risk assessment.

2. Materials and methods

2.1. Cell culture and chemical exposure

Human immortalized keratinocyte cells (HaCaT) were obtained from Enzyme Research Biotechnology Co., Ltd. (Shanghai, China). Cells were cultured in Dulbecco's Modified Eagle Medium (DMEM) supplemented with 10% fetal bovine serum (FBS) and 1% penicillin–streptomycin. Cells were maintained at 37 °C in a humidified incubator with 5% CO_2. For exposure experiments, cells were seeded and allowed to attach for 24 h before treatment. During exposure, cells were cultured in DMEM containing 0.1% FBS. Cells were exposed to individual OPEs or their mixtures for 48 h. Three OPEs, including tributyl phosphate (TNBP), triphenyl phosphate (TPHP), and tris (1, 3-dichloro-2-propyl) phosphate (TDCIPP), were chosen as tested chemicals, and Table S1 summarizes their basic information.

All solvents and reagents were of high-performance liquid chromatography (HPLC) grade. TDCIPP (93%) and TPHP (99%) were purchased from J&K Scientific (Beijing, China), and TNBP (99%) was obtained from Macklin Biochemical Co., Ltd. (Shanghai, China). Stock solutions were prepared in dimethyl sulfoxide (DMSO) and diluted with culture medium to the desired concentrations before exposure. The final concentration of DMSO in all treatments was maintained at $\leq$ 0.1% (v/v).

2.2. Cytotoxicity assay and dose–response curve fitting

Cell viability was determined using a Cell Counting Kit-8 (CCK-8, Biosharp, China). HaCaT cells were seeded in 24-well plates at a density of 1.4×10^6 cells per well. After 48 h of exposure, CCK-8 solution was added to each well at a ratio of 1:100 (v/v) and incubated for 2 h. Absorbance was measured at 450 nm using a VARIOSKAN LUX microplate reader (Thermo Fisher Scientific, USA). Cell viability was calculated as:

$$\text{Cell viability } (\%) = \frac{A_{sample} - A_{blank}}{A_{control} - A_{blank}} \times 100$$

All experiments were performed with at least three independent

replicates. Concentrations were log-transformed before fitting. Nonlinear regression was then performed using a four-parameter logistic model, and EC_{10}, EC_{20}, EC_{50}, and EC_{80} were derived from the fitted log-concentration–cell viability curves.

2.3. Mixture design and combination index (CI) analysis

Binary and ternary mixtures were prepared based on predefined molar ratios (1:4, 1:1, and 4:1 for binary mixtures; multiple ratios for ternary mixtures were summarized in Tables S2-S3). For fixed-ratio mixtures, the mixture concentration used for dose–response fitting and CI analysis was expressed as the total molar concentration, defined as the sum of the molar concentrations of all components. The concentration of each individual component was determined by its predefined molar fraction in the mixture. All concentrations used in the dose–response and CI analyses were expressed on a molar basis. Notably, the mixture ratios were selected to compare component-dominated and equal-ratio conditions, thereby covering different composition scenarios and identifying composition-dependent changes in interaction patterns. Mixture toxicity was evaluated using the Chou–Talalay method based on at least three independent experiments for each concentration. Dose–effect relationships for individual OPEs and fixed-ratio mixtures were fitted using the median-effect equation in CompuSyn, from which the median-effect dose (Dm), slope parameter (m), standard error of m, and correlation coefficient (r) were obtained (Table S4). At each fraction affected (Fa), the fitted median-effect relationships were used to estimate the corresponding single-compound doses (Dx) and calculate the combination index (CI). The equation is:

$$CI = \sum \frac{D_i}{D_{xi}}$$

where D_i represents the dose of each compound in the mixture and D_{xi} is the dose of the compound alone that produces the same effect. $CI < 1$, $CI = 1$, and $CI > 1$ were interpreted as synergism, additivity, and antagonism, respectively. CI–Fa profiles and isobolograms were generated to characterize interaction patterns across effect levels. The variability of CI estimates was further evaluated using Sequential Deletion Analysis (S.D.A.) in CompuSyn, and the resulting statistics are summarized in Table S5. S.D.A.-derived intervals entirely below or above $CI = 1$ were considered supportive of synergism or antagonism, respectively, whereas intervals spanning $CI = 1$ were considered compatible with additivity. Detailed procedures for median-effect fitting, CI calculation, isobologram analysis, and S.D.A. are provided in **Text S1** of the Supplementary data.

2.4. Barrier permeability assay

Cellular barrier integrity was evaluated using a Transwell system with FITC-dextran. HaCaT cells were seeded in 12-well Transwell inserts at a density of 1.5×10^5 cells/cm^2. Control and OPE-treated cells were maintained under identical serum conditions and comparable confluence during the exposure period. The ternary mixture was prepared at a fixed TNBP:TPHP:TDCIPP molar ratio of 1:1:1, with total nominal molar concentrations of 0.1, 1, and 10 μM, corresponding to 0.033, 0.333, and 3.33 μM of each component, respectively. After 48 h of exposure, 500 μL FITC-dextran (2 mg/mL, diluted in serum-free DMEM) was added to the apical chamber, while 1 mL serum-free DMEM was added to the basolateral chamber. After 2 h incubation, fluorescence intensity was measured at excitation/emission wavelengths of 488/518 nm using a microplate reader.

2.5. Gene expression analysis

Total RNA was extracted using TRIzol reagent and quantified using a NanoDrop spectrophotometer. cDNA was synthesized using the Evo M-MLV reverse transcription kit (Accurate Biology, China). Quantitative real-time PCR (qPCR) was performed using the SYBR Green Pro Taq HS kit. Gene-specific primers (Table S6) were synthesized by Tsingke Biotechnology (Beijing, China). Gene expression levels were normalized to β-actin and calculated using the $2^{-}\Delta\Delta Ct$ method. β-actin showed stable expression across all experimental groups, with Cq values ranging from 14.79 to 15.53 and no significant differences among groups ($p = 0.171$).

2.6. Metabolite extraction and QA/QC

To control for the potential effects of serum conditions on cellular metabolism, control and OPE-treated cells were maintained under identical culture conditions, and treatment effects were evaluated relative to the matched control group. Following 48 h of exposure, cells were washed twice with cold PBS and harvested. Cell pellets were extracted with 500 μL methanol/water (1:1, v/v) containing internal standards. Samples were vortexed, subjected to three freeze–thaw cycles, and centrifuged at 12,000 rpm for 10 min at 4 °C. The supernatant was collected and further processed for analysis. Quality control (QC) samples were prepared by pooling aliquots from all samples and injected every 10 runs to correct the mass, retention time, and response drift.

2.7. Untargeted metabolomics analysis

For metabolomic analysis, individual OPE exposures were conducted at 10 μM per compound, whereas mixture exposures were conducted at a total nominal molar concentration of 10 μM. Binary and ternary mixtures were prepared using equal molar ratios. The same total concentration was used across all exposure groups to facilitate direct comparison of composition-dependent metabolic responses, and cell viability remained above 90% under these conditions. Untargeted metabolomics analysis was performed using a Vanquish ultrahigh-performance liquid chromatography system coupled to a Q Exactive HF-X mass spectrometer (Thermo Scientific) in both positive and negative electrospray ionization modes. Chromatographic separation was achieved using an ACQUITY Premier HSS T3 column (1.8 μm, 2.1 × 100 mm; Waters) with water and acetonitrile containing 0.1% formic acid as the mobile phases. Mass spectra were acquired over m/z 75–1000 using data-dependent acquisition with stepped collision energies. Detailed chromatographic gradients, ion-source settings, acquisition parameters, and other instrumental conditions are provided in **Text S2** of the Supplementary data.

Raw mass spectrometry data were converted to mzXML format using MSConvert. Data processing, including peak detection, alignment, and retention time correction, was performed using XCMS. Missing values (> 50%) were removed, and remaining missing values were imputed using KNN. Data normalization was performed using support vector regression (SVR). The analytical stability of the LC–MS/MS platform was further evaluated by correlation analysis of QC samples (Figure S1), with all pairwise correlation coefficients showing $|r| > 0.99$, confirming high analytical stability across the sequence. Metabolites were annotated based on accurate mass and MS/MS spectral matching against HMDB, KEGG, and METLIN databases. Only metabolites with a metabolite annotation score > 0.5 and a coefficient of variation < 0.30 in QC samples were retained for subsequent analysis. PCA was initially performed as an unsupervised method to visualize the overall data structure, and the tight clustering of QC samples confirmed the stability and reproducibility of the analytical platform. Differential metabolites were screened using VIP > 1, $p < 0.05$, and fold change (FC) < 0.8 or > 1.2. The p-values were additionally adjusted using the Benjamini–Hochberg false discovery rate (FDR) procedure.

2.8. Statistical analysis

All data are presented as mean ± standard deviation (SD). Statistical

significance was assessed using one-way ANOVA followed by Dunnett's multiple-comparisons test. Differences were considered statistically significant at $p < 0.05$.

3. Results and discussion

3.1. Dynamic shifts in OPE mixture interactions

Chemical mixture toxicity is commonly characterized by classifying interactions as synergistic, additive, or antagonistic. However, such classifications generally assume that interaction patterns represent relatively stable properties of chemical combinations, whereas whether mixture responses dynamically change under different exposure conditions remains insufficiently understood. To characterize the interaction patterns within OPE mixtures (TNBP, TPHP, TDCIPP), the combined effects of OPE mixtures with varying ratios were evaluated on HaCaT cells based on cytotoxicity data (Figures S2-S5 and Tables S7-S9), and combination index (CI) values were calculated across a continuous range of fraction affected (Fa) values. Non-additive effects, including synergistic (CI < 1, greater than additive) and antagonistic (CI > 1, less than additive) interactions, were then used to characterize the mixture responses [28]. Before interpreting the interaction profiles, the reliability and variability of the underlying dose–effect models were evaluated. The median-effect analyses yielded r values of 0.8223–0.9971, with 16 of the 19 fitted profiles showing r ≥ 0.90, indicating generally good model–data agreement despite some variation in fitting performance (Table S4). S.D.A.-based analysis further showed that CI variability differed across Fa values, with CI estimates close to 1 more frequently associated with uncertainty intervals spanning the additivity boundary (Table S5).

The ternary OPE mixtures exhibited substantial non-additive responses across different combination ratios. Most ternary OPE mixtures exhibited synergistic interactions over broad Fa ranges after S.D.A.-based uncertainty was considered. As shown in Fig. 1, the mixture with TNBP: TPHP: TDCIPP ratios of 1:1:1 and 4:1:4 remained synergistic throughout the Fa range. However, the interaction profiles varied across effect levels and mixture compositions. The mixtures with TNBP: TPHP: TDCIPP ratios of 1:4:4 and 1:4:1 showed uncertainty intervals compatible with additivity at lower Fa values, followed by clear synergism from Fa ≥ 0.25 and Fa ≥ 0.30, respectively, indicating progressively strengthened synergistic responses. In contrast, the 4:1:1, 4:4:1, and 1:1:4 mixtures remained synergistic over low-to-intermediate Fa ranges, but became compatible with additivity at Fa ≥ 0.90, 0.95, and 0.90, respectively.

These results suggested that the interaction profiles of OPE mixtures could vary across mixture compositions and effect levels, although the extent of these variations was subject to uncertainty in CI estimation. Previous mixture toxicity studies have primarily focused on identifying whether chemical combinations produce synergistic, additive, or antagonistic effects, whereas the potential transition between different interaction modes has received considerably less attention [29,30]. For example, zhang et al. identified the binary combined effects between 13 environmental organic compounds on HepG2 cells [11]. Similarly, Lola Bajard et al. reported that co-exposure to these flame retardants might induce additive anti-androgenic activity [31]. And the observed dynamic interaction trajectories indicated that mixture toxicity could not be adequately represented by a single interaction category and may introduce additional uncertainty into conventional mixture risk assessment approaches. Therefore, the key challenge in evaluating chemical mixtures is not only identifying whether synergism or antagonism occurs, but also understanding the factors controlling the transition between different interaction states. These findings motivated further investigation into whether individual OPE components contribute differently to mixture toxicity and determine the direction of interaction outcomes.

3.2. Opposing roles of OPE components in mixture toxicity

The dynamic interaction patterns observed in ternary mixtures raised an important question: whether individual components contribute equally to mixture toxicity or whether specific chemicals play distinct functional roles in shaping overall responses. To address these questions, binary combinations among TNBP, TPHP, and TDCIPP were further evaluated using CI analysis and isobologram approaches (**Figures 2A-2L** and **S6**). The TNBP-TPHP combination exhibited a concentration-dependent transition between interaction modes, with synergistic effects observed at lower effect levels and antagonistic responses emerging at higher effect levels. In contrast, the TPHP-TDCIPP combination consistently displayed synergistic interactions across different effect levels, with data points remaining within the synergistic region of the isobologram. Conversely, the TNBP-TDCIPP combination showed predominantly antagonistic interactions, with the antagonism attenuating slightly as the effect level of the TNBP–TDCIPP mixture increased. Therefore, distinct interaction behaviors observed among different binary combinations suggested that individual component contributions might vary under different combinations. Especially at lower effect levels (e.g., EC_{10} and EC_{20} in Figs. 2**A**-2**B** and 2**I-2J**), the TPHP–TDCIPP combination was synergistic whereas the TNBP–TDCIPP combination was antagonistic, potentially indicating that TNBP and TPHP elicited opposite interaction modes when combined with TDCIPP. Furthermore, comparison of individual cytotoxicity further revealed different toxicity levels among the three OPEs (Figure S7 and Table S7), with TPHP exhibiting the strongest cytotoxicity, followed by TDCIPP and TNBP. These differences in toxicity among the three OPEs might potentially contribute to the distinct interaction patterns observed when TNBP or TPHP was combined with TDCIPP, potentially suggesting that individual component properties should be considered together with specific pairing context when interpreting mixture response.

This observation highlights an important aspect of chemical mixture toxicity: individual components may act not only as toxic contributors but also as interaction modifiers that reshape the overall biological response of the mixture. Such component-specific roles may help explain why chemical mixtures containing similar compounds can generate highly variable toxicity outcomes. Previous studies have suggested that structurally distinct OPEs may activate different cellular pathways, including oxidative stress responses, lipid metabolism disturbances, and

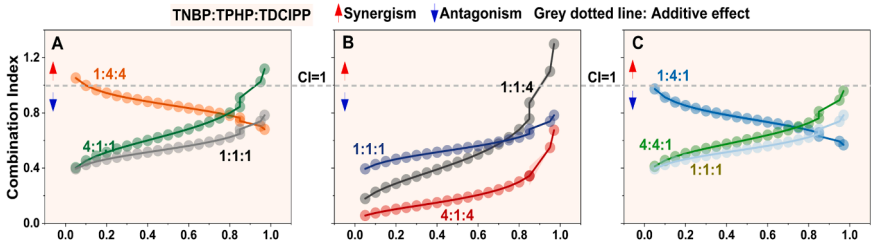


Fig. 1. Combination index (CI–Fa) plot for seven mixture ratios of the three OPEs (A–C). CI values are plotted as a function of the fraction affected (Fa) by computer simulation (CompuSyn). CI < 1, = 1, and > 1 indicate synergism, additive effects, and antagonism, respectively.

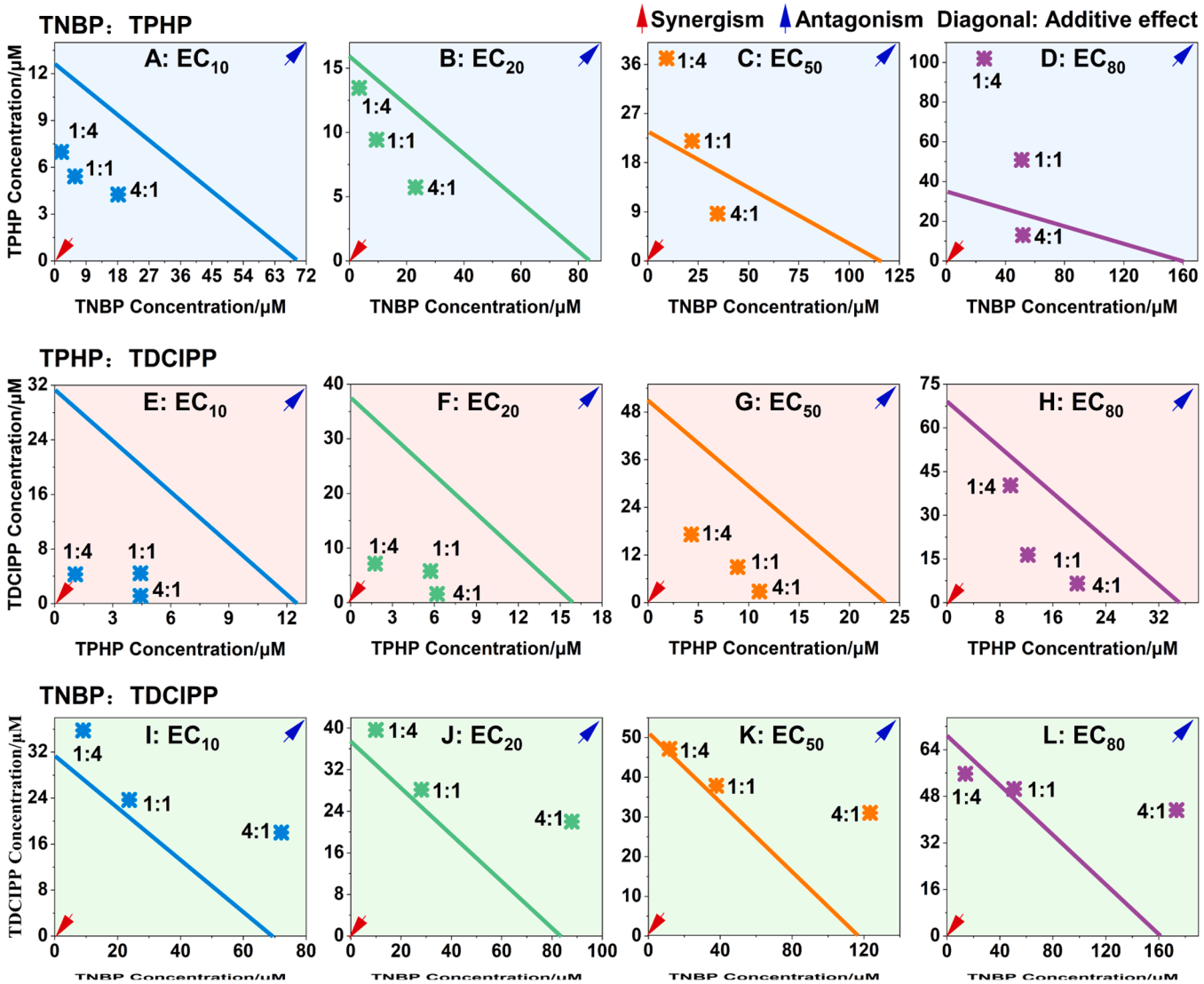


Fig. 2. Isobolograms for the binary combinations of TNBP, TPHP, and TDCIPP at different cytotoxicity levels (A-L). The x- and y-axes represent the concentrations of the two components in each mixture, respectively. In each panel, the colored diagonal line indicates the concentration-addition response. Regions in the direction of the red arrows denote synergistic effects, whereas regions in the direction of the blue arrows denote antagonistic effects.

nuclear receptor signaling [18]. For instance, TNBP and TDCIPP have been reported to induce excessive reactive oxygen species (ROS) production in HepG2 cells, whereas TPHP showed a different response pattern [32]. Other studies further suggested that TDCIPP and TPHP might involve distinct mechanisms in neurotoxicity, reproductive toxicity, and hepatotoxicity [33]. And the combination of TDCIPP and TPHP has been reported to enhance the biological activities of liver X receptor and nuclear factor erythroid 2-related factor 2, which may partially explain the strong synergistic interaction observed in their combined exposure [11]. Therefore, differences in biological perturbation patterns among individual OPE components may provide a mechanistic basis for their opposing influences on mixture toxicity. Collectively, these findings indicate that mixture toxicity is not simply determined by the sum of individual chemical potencies. Instead, specific components may disproportionately influence interaction outcomes through their distinct biological responses, emphasizing the need to identify key functional contributors within complex chemical mixtures.

3.3. *OPE mixtures impair skin barrier integrity*

While mixture interaction analysis revealed dynamic shifts in toxicity responses, understanding whether this interaction pattern translates into biologically relevant consequences is essential for evaluating health implications. The skin represents a critical exposure interface for environmental contaminants, functioning not only as a physical barrier but also as a regulator of chemical penetration and internal susceptibility [34]. Therefore, we further investigated whether OPE mixture exposure could alter barrier-associated responses in HaCaT cell monolayers. Given the limited comparability of concentrations reported in wipe samples (ng/handwipe), human biomonitoring data from internal exposure matrices were used to contextualize the lower experimental concentration (Table S10) [17,19]. The total nominal molar concentration of 0.1 μM, corresponding to 0.033 μM of each component, was selected to approximate the upper range of reported internal exposure levels, whereas 1 and 10 μM were included as exploratory higher in vitro exposure levels while maintaining cell viability above 90%. These concentrations represent the total nominal concentrations of the ternary mixture, with TNBP:TPHP:TDCIPP fixed at 1:1:1, corresponding to individual component concentrations of 0.033, 0.333, and

3.33 μM at total mixture concentrations of 0.1, 1, and 10 μM, respectively. The CI values of these concentrations were < 1 according to CI–Fa profiles. Following exposure to ternary OPE mixtures, FITC-dextran permeability assays were performed to evaluate changes in HaCaT monolayer permeability. Increased FITC-dextran transport from the apical to basolateral compartment was observed following OPE mixture exposure, with significant increases detected at the intermediate and highest nominal concentrations (Fig. 3**A-3D**). The calculated permeability coefficients further demonstrated a concentration-dependent increase, indicating increased monolayer permeability. In addition to changes in permeability, OPE mixtures altered the expression patterns of genes involved in epidermal differentiation. Early differentiation markers, including KRT1, KRT10, and IVL, were upregulated, whereas terminal differentiation-associated markers, including FLG and LOR, were downregulated following OPE exposure (Fig. 3**E**). These changes suggest that OPE mixtures altered keratinocyte differentiation-related responses and may interfere with the formation and maintenance of epidermal barrier-associated functions. Altered expression of AQP3 further indicated potential disturbance of water transport regulation, which is essential for maintaining epidermal homeostasis. However, the HaCaT transwell monolayer represents a simplified barrier model and does not reproduce the full three-dimensional structure and functional complexity of the human epidermis; therefore, these findings primarily reflect barrier-associated cellular responses under the present experimental conditions.

The skin barrier serves as the first biological interface controlling the transition of external chemical exposure into internal biological responses [35]. Therefore, mixture-induced barrier impairment may have implications beyond local cellular toxicity by modifying the relationship between external exposure levels and effective internal susceptibility. This consideration is particularly relevant for chemical mixtures because differential permeability among individual components may further alter the actual composition reaching target cells [36]. On the one hand, TNBP, TPHP, and TDCIPP exhibited different dermal penetration coefficients (5.00×10^{-4}, 4.70×10^{-5}, and 1.26×10^{-4} cm/hour, respectively) [14], barrier disruption might lead to differential penetration efficiencies among components and consequently modify the effective mixture composition reaching skin cells. On the other hand, biomonitoring studies also reported substantially higher dermal exposure levels of TPHP than those of TNBP and TDCIPP. Handwipe measurements among workers showed 1181 ng/handwipe for TPHP, compared with 3.96 and 57.2 ng/handwipe for TNBP and TDCIPP, respectively [17]. Similarly, studies in the general population reported 112 ng/m^2 for TPHP, compared with 12.6 and 41.3 ng/m^2 for TNBP and TDCIPP [14]. In the present study, TPHP-rich mixtures (TNBP:TPHP:TDCIPP = 1:4:1) also showed progressively enhanced synergistic interactions with increasing Fa, highlighting the potential relevance of TPHP-rich co-exposure scenarios to dermal risk assessment. Consequently, disruption of barrier function may introduce additional uncertainty into dermal risk assessment, especially when mixture toxicity depends strongly on component interactions. Although the present study used a simplified HaCaT-based ternary mixture system, whereas real human dermal exposure involves more complex skin structures, penetration kinetics, and mixture compositions, the controlled experimental design provides a useful basis for identifying composition-dependent interaction patterns. These findings therefore provide useful mechanistic insight into how OPE mixtures may affect the biological interface regulating dermal exposure and offer guidance for future studies of complex dermal mixture exposure and risk assessment.

3.4. Lipid metabolic remodeling associated with component-specific toxicity responses

The opposing roles of OPE combination in mixture toxicity suggested that differences in biological perturbation patterns may contribute to the observed interaction behaviors. Because membrane lipid composition is essential for maintaining epithelial structure, permeability, and cellular signaling [37], we further investigated whether lipid metabolic remodeling could provide mechanistic insights into component-specific toxicity responses. PCA showed tight clustering of QC samples in both ionization modes, supporting analytical stability (Figure S8). PLS-DA further revealed clear separation among the control and OPE-exposed groups, and the 200-permutation tests further supported model validity, with R^2Y/Q^2 values of 0.988/0.882 for ESI^+ and 0.979/0.867 for ESI^- (Figure S9).

Among all exposure groups, 170, 419, 524, 526, 410, 483, and 526 differential metabolites were identified in the TNBP, TPHP, TDCIPP, TNBP–TPHP, TNBP–TDCIPP, TPHP–TDCIPP, and TNBP–TPHP–TDCIPP groups, respectively (Fig. 4**A-4G**). Notably, lipid-related metabolites represented a major proportion of altered metabolic features across all exposure groups (Fig. 4**H**), suggesting that lipid homeostasis represents a sensitive metabolic target of OPE exposure. Further lipidomic analysis revealed that altered lipids mainly belonged to fatty acyls (FA), glycerolipids (GL), glycerophospholipids (GP), and sphingolipids (SP) (**Figures 5** and **S10**), which participate in membrane organization, energy storage, and cellular signaling [38,39]. Among these lipid classes, GP showed particularly prominent alterations (Table S11). TNBP, TPHP, TDCIPP, TNBP–TPHP, TNBP–TDCIPP, TPHP–TDCIPP, and TNBP–TPHP–TDCIPP exposure altered 58, 105, 85, 104, 87, 105, and 105 glycerophospholipid species, respectively (Fig. 5). Consistently, glycerophospholipid metabolism was the most significantly enriched pathway across these exposure groups, with rich factors of 0.21, 0.36, 0.27, 0.37, 0.28, 0.35, and 0.33, respectively (Figures S11-S17). Notably, under equal-ratio binary exposure at a total nominal molar concentration of 10 μM, TNBP–TPHP and TPHP–TDCIPP exhibited synergistic effects, whereas TNBP–TDCIPP was compatible with additivity. Although all exposure groups were significantly enriched in the glycerophospholipid metabolism pathway, the TNBP–TDCIPP combination showed relatively weaker enrichment of glycerophospholipid metabolism than TNBP–TPHP and TPHP–TDCIPP. These suggest that differences in glycerophospholipid metabolic perturbation may be associated with their distinct interaction patterns.

Furthermore, GPs, including phosphatidylcholine (PC) and phosphatidylethanolamine (PE), are major structural components of cellular membranes and contribute to membrane stability and permeability regulation [40]. Multiple PC and PE species showed increased levels across all exposure groups (Fig. 6). In particular, enrichment of long-chain unsaturated PC and PE species suggested potential alterations in membrane lipid organization because unsaturated fatty acyl chains generally reduce lipid packing and increase membrane fluidity [41–45]. In addition, increased lysophosphatidylethanolamine (LPE) levels following OPE exposure indicated enhanced phospholipid turnover, further reflecting membrane lipid remodeling responses [46,47]. Together, these lipid alterations provide a potential mechanistic interpretation for the barrier impairment observed after OPE exposure. Rather than representing isolated metabolic changes, lipid remodeling may reflect cellular adaptation responses to chemical-induced membrane stress and may contribute to differences in biological susceptibility among OPE components.

3.5. Distinct lipid signatures of OPE components

Lipid homeostasis is a highly dynamic regulatory process modulated by multiple interconnected pathways, including energy storage, membrane lipid turnover, oxidative stress, and cellular signaling [48]. Although all exposure groups affected lipid homeostasis, individual and combined exposures showed distinct lipid response patterns. Network reconstruction of glycerolipid and glycerophospholipid metabolism revealed compound-specific remodeling patterns (Fig. 7). Glycerolipid and glycerophospholipid metabolism were markedly altered across all exposure groups, with increased levels of diacylglycerol (DG) and triacylglycerol (TG). These increases were more pronounced in the

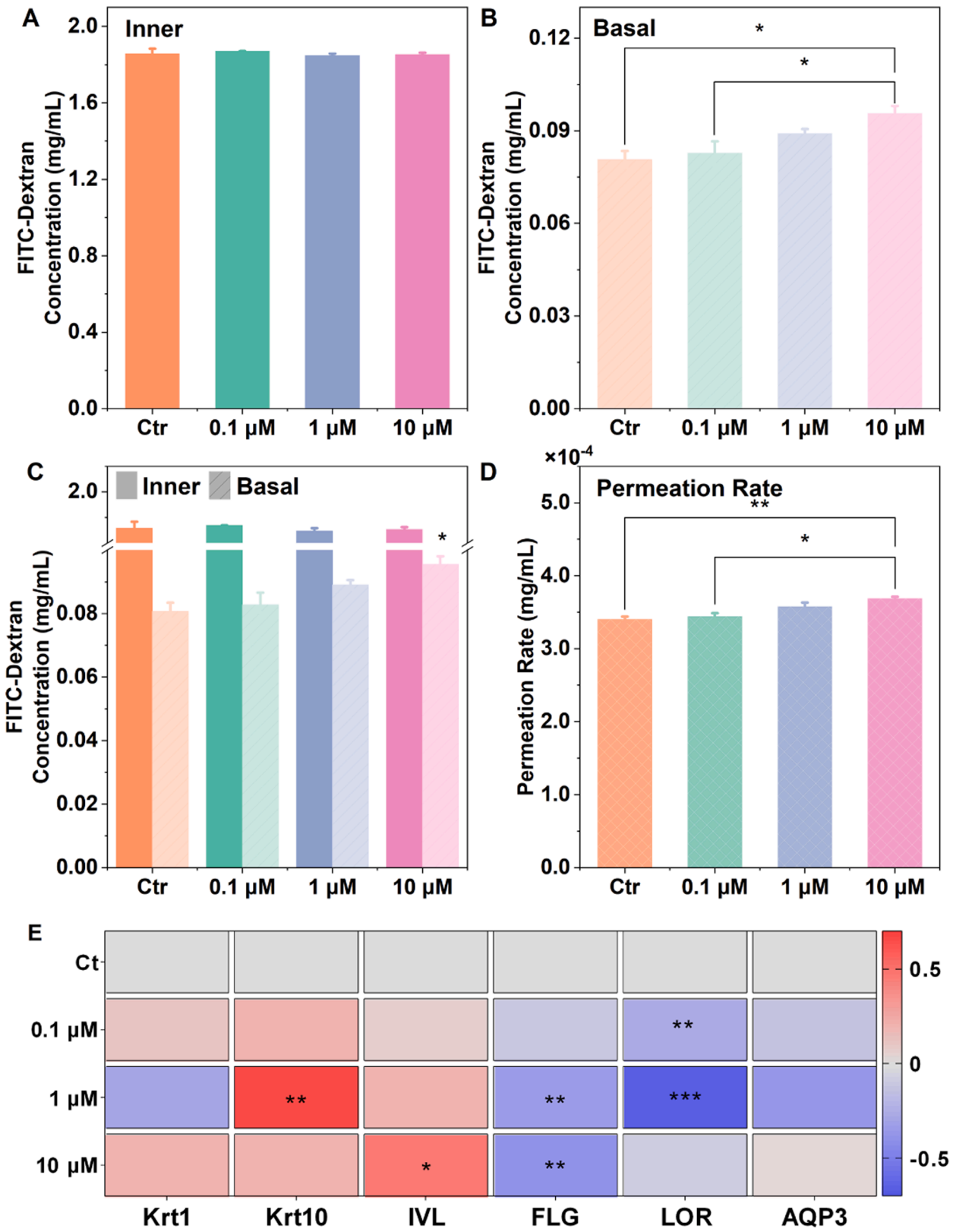


Fig. 3. Changes in HaCaT cell permeability (A-D) and transcriptional expression of key genes involved in epidermal differentiation induced by combined OPEs exposure (E). (A, B) FITC-dextran concentrations in the upper and lower chambers of the Transwell system, respectively. (C) Comparison of FITC-dextran concentrations between the upper and lower chambers of the Transwell system. (D) Permeability of HaCaT cells after exposure to different concentrations of OPEs. The concentrations of 0.1, 1, and 10 μM represent the total nominal concentrations of the ternary mixture, with TNBP:TPHP:TDCIPP fixed at 1:1:1, corresponding to individual component concentrations of 0.033, 0.333, and 3.33 μM at total mixture concentrations of 0.1, 1, and 10 μM, respectively. Data are presented as the mean of at least three independent experiments. $^{*}p < 0.05$, $^{**}p < 0.01$, $^{***}p < 0.001$, $^{****}p < 0.0001$.

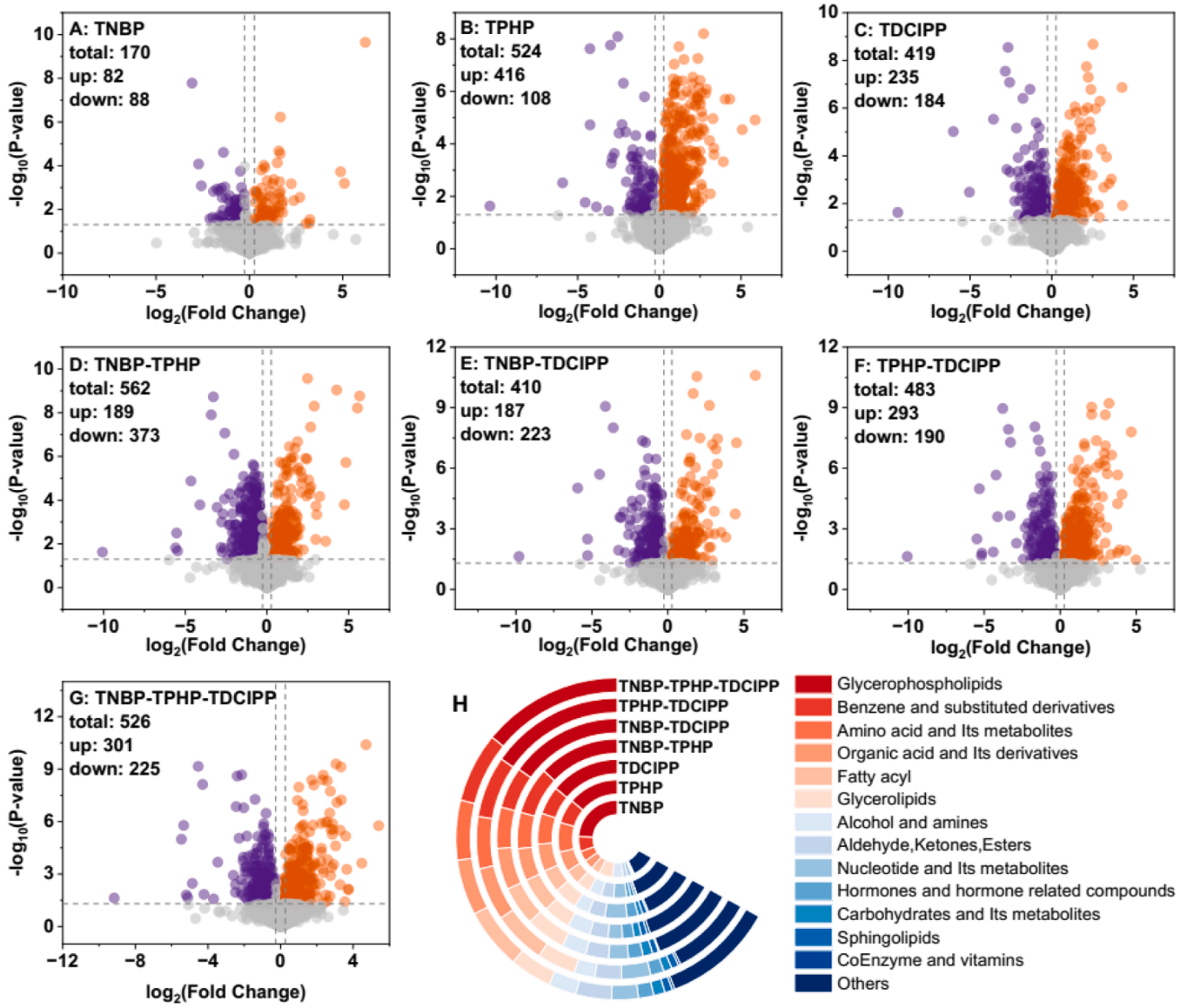


Fig. 4. Differential metabolite analysis in HaCaT cells after 48 h of OPE exposure: volcano plots (A-G), and donut charts of metabolite class distribution (H). Metabolites with VIP > 1, FC < 0.8 or > 1.2, and $p < 0.05$ were defined as significantly altered. In the volcano plots, orange circles indicate upregulated metabolites, purple circles indicate downregulated metabolites, and gray circles indicate metabolites with no significant difference.

TNBP–TDCIPP, TPHP–TDCIPP, and TNBP–TPHP–TDCIPP groups, which were compatible with additivity, synergism, and synergism, respectively, according to the corresponding CI–Fa profiles. Within the glycerolipid metabolic branch, DG and TG serve as critical intracellular lipid storage forms while also participating in membrane biogenesis and cell signal transduction [49]. In contrast, oxidized lipids showed a different response pattern. Their levels increased following individual TPHP and TDCIPP exposure but were lower following TNBP and combined exposures. Lipid peroxides are typically detrimental to cellular membranes, as they alter bilayer thickness, permeability, and structural stability, and are closely associated with pathological conditions such as skin inflammation and psoriasis [27,50]. The increased oxidized lipid levels following TPHP and TDCIPP exposure therefore indicate enhanced lipid oxidative stress. In comparison, the accumulation of DG and TG together with lower oxidized lipid levels downstream under combined exposure suggests that the additive or synergistic responses were accompanied by a redistribution of lipid metabolism among storage, oxidation, and membrane lipid remodeling rather than a simple amplification of the responses induced by individual compounds. Consistent with this pattern, PC, PE, phosphatidic acid (PA), phosphatidylglycerol (PG), and phosphatidylinositol (PI) were increased in most mixture groups, suggesting enhanced involvement of glycerolipid intermediates in downstream glycerophospholipid metabolism and membrane lipid remodeling. Besides, phosphatidylserine (PS) also increased markedly in most mixture groups. PS is one of the most abundant negatively charged phospholipids on the inner leaflet of mammalian cellular membranes, participating in fundamental processes including membrane trafficking, cell signaling, and membrane structure regulation [51]. Additionally, PS is considered to possess antioxidant functions, particularly in counteracting phospholipid membrane lipid peroxidation [52]. The concurrent increase in PS and decrease in oxidized lipids observed in several mixture groups may therefore reflect a compensatory phospholipid remodeling response associated with membrane stabilization and regulation of oxidative stress. Collectively, these findings indicate that mixture exposure was accompanied by a reorganization of the lipid response patterns observed after individual exposure rather than a simple addition of the effects of the individual components.

Further comparison of the binary mixtures revealed that specific

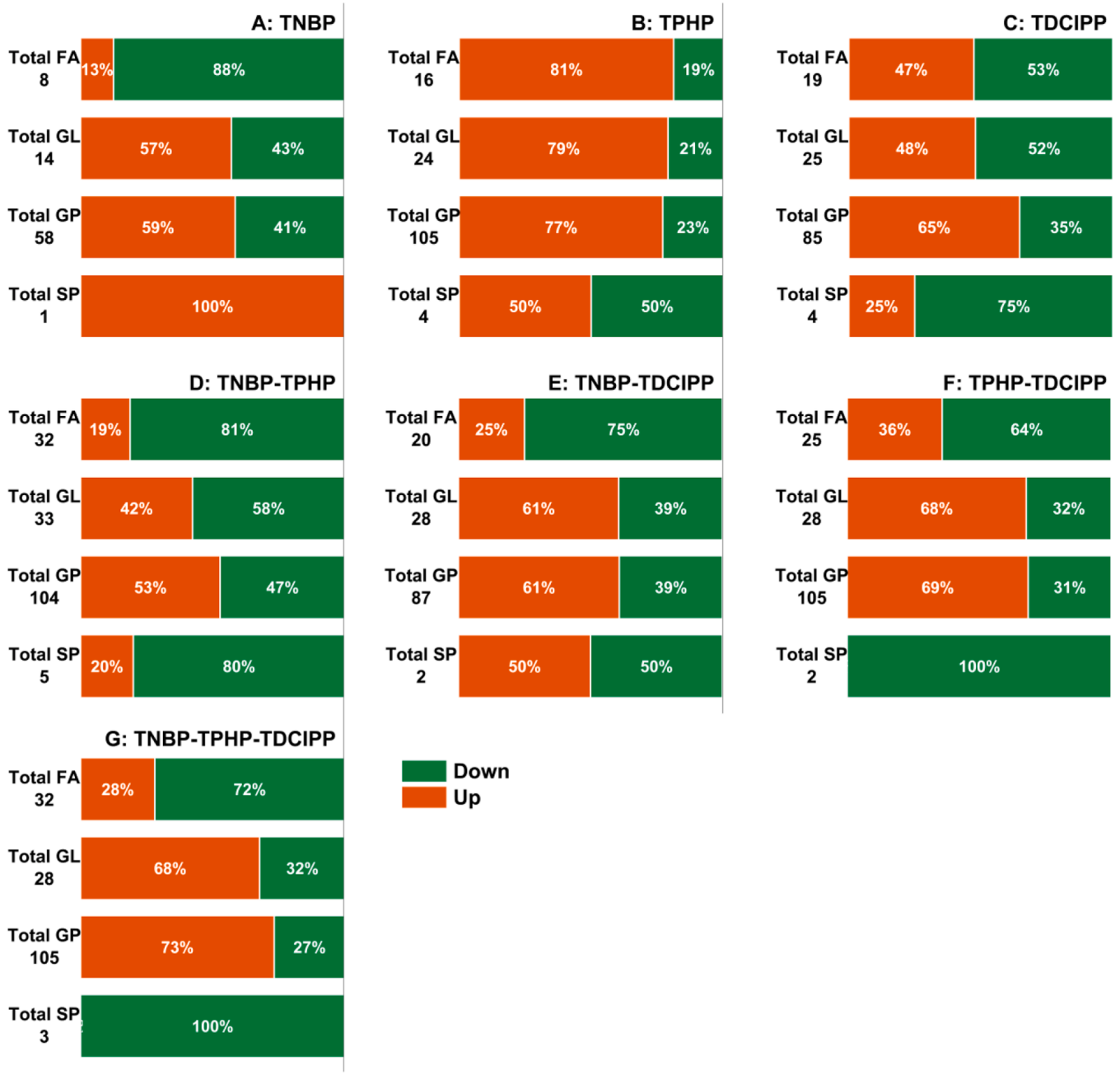


Fig. 5. Metabolic alterations following OPE exposure in HaCaT cells. Proportions of upregulated versus downregulated metabolites across various lipid subclasses (A–TNBP, B–TPHP, C–TDCIPP, D-TNBP-TPHP, E-TNBP-TDCIPP F-TPHP-TDCIPP, G-TNBP-TPHP-TDCIPP). FA, GL, GP, and SP represent fatty acyls, glycerolipids, glycerophospholipids, and sphingolipids, respectively.

glycerophospholipid subclasses exhibited distinct response patterns associated with different interaction states. Under equal-ratio binary exposure at a total nominal molar concentration of 10 μM, TNBP–TPHP and TPHP–TDCIPP exhibited synergistic effects, whereas TNBP–TDCIPP was compatible with additivity. Although all three binary mixtures significantly perturbed glycerophospholipid metabolism, lysophosphatidylcholine (LPC) showed a particularly distinct response (Fig. 7). LPC levels increased by approximately sevenfold and more than sixfold in the TNBP–TPHP and TPHP–TDCIPP groups, respectively, but decreased to approximately 0.5-fold in the TNBP–TDCIPP group (Figure S18). LPC is an important lysophospholipid generated from phosphatidylcholine and participates in membrane phospholipid turnover, membrane remodeling, and cellular signaling responses [53]. The pronounced LPC increases in the two synergistic combinations may therefore reflect more extensive phospholipid turnover and remodeling, whereas the opposite LPC response in TNBP–TDCIPP further demonstrates that different combinations can generate distinct lipid perturbation patterns. Notably, both synergistic combinations contained TPHP and showed strongly enhanced LPC responses, whereas the TNBP–TDCIPP combination showed a different response direction. These findings suggest that individual components may reshape the overall lipid response in a mixture-dependent manner and thereby contribute differently to the resulting biological perturbation. Mixture toxicity therefore cannot be inferred simply from individual chemical potency or metabolic responses, but may also depend on the specific biological perturbation patterns generated by different component combinations.

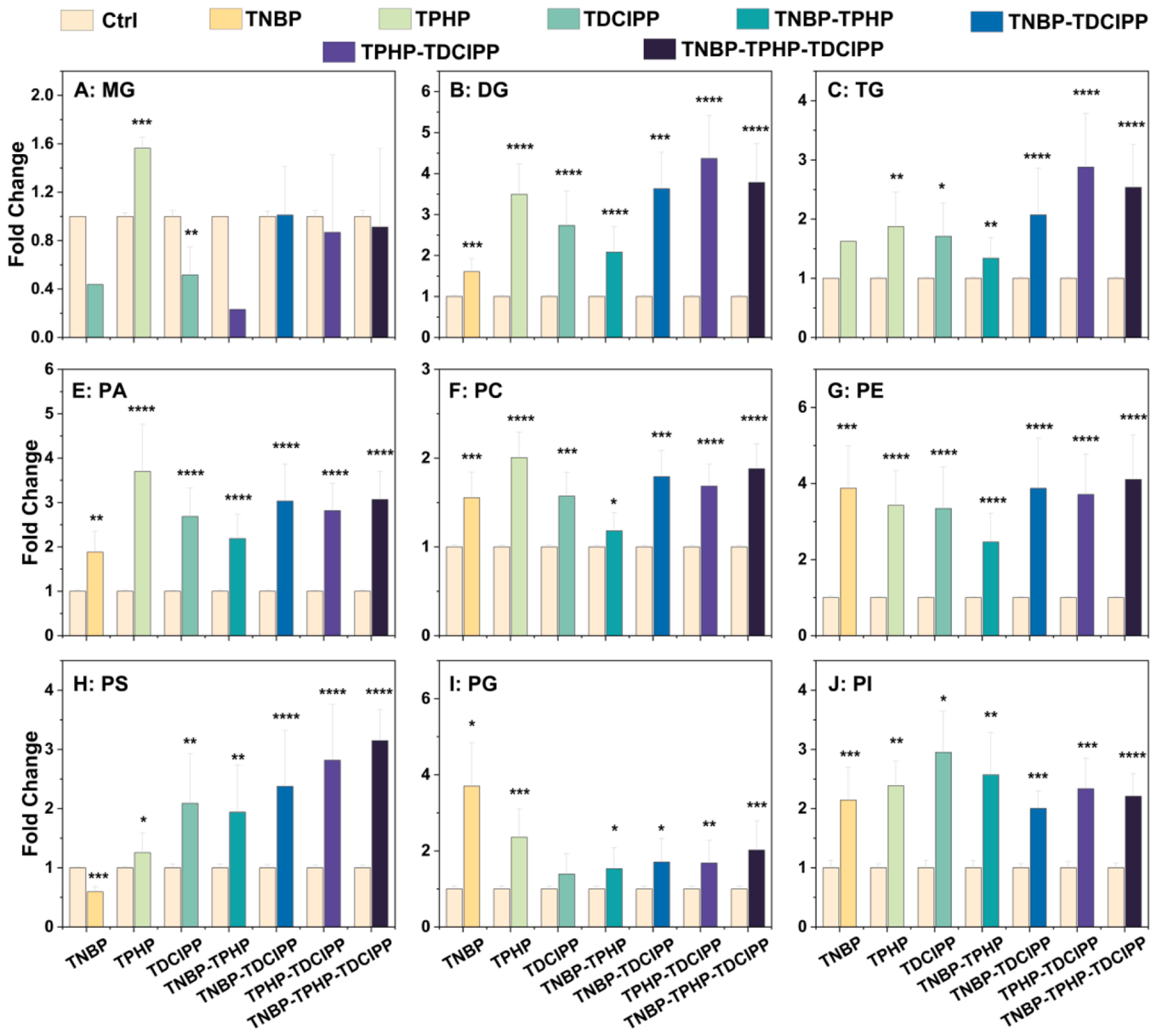


Fig. 6. Perturbations in lipid metabolism and fold changes of different lipid classes (n = 6) in HaCaT cells after 48 h individual and combined OPE exposures. MG, DG, TG, PA, PC, PE, PS, PG, and PI represent monoacylglycerols, diacylglycerols, triacylglycerols, phosphatidic acid, phosphatidylcholine, phosphatidylethanolamine, phosphatidylserine, phosphatidylglycerol, and phosphatidylinositol, respectively. Error bars represent the SEM, and no error bars are shown for classes with fewer than two metabolites. $^{*}p < 0.05$, $^{**}p < 0.01$, $^{***}p < 0.001$, $^{****}p < 0.0001$.

3.6. *Implications for mechanism-informed mixture risk assessment*

Chemical risk assessment has traditionally relied on evaluating individual substances based on their exposure levels and intrinsic toxicity [54–56]. However, the present study demonstrates that mixture toxicity cannot always be inferred from individual chemical effects because different component combinations can produce distinct interaction outcomes. The composition- and effect-level-dependent changes in interaction strength and mode observed in OPE mixtures indicate that mixture effects should not be considered as fixed characteristics of chemical combinations. Instead, interaction outcomes may vary depending on mixture composition and biological response states. Identification of components whose presence or relative abundance is consistently associated with changes in mixture behavior may provide valuable information for prioritizing chemicals within complex exposure scenarios. Accordingly, chemical prioritization could consider not only exposure level and intrinsic hazard, but also the potential of a chemical to modify the combined effects of co-occurring contaminants. From a mixture-management perspective, combinations showing persistent or pronounced non-additive interactions could be prioritized for targeted monitoring and mixture-specific toxicity evaluation. Furthermore, the association between component-specific toxicity responses and lipid metabolic remodeling highlights the potential value of integrating mechanism-relevant biological information into mixture risk assessment. Rather than relying solely on external concentrations or individual chemical toxicity data, future assessment frameworks may benefit from incorporating interaction dynamics and biological response signatures to better characterize risks arising from complex chemical mixtures. Such information may help identify mixture combinations that warrant greater regulatory attention and support more targeted management of co-occurring contaminants.

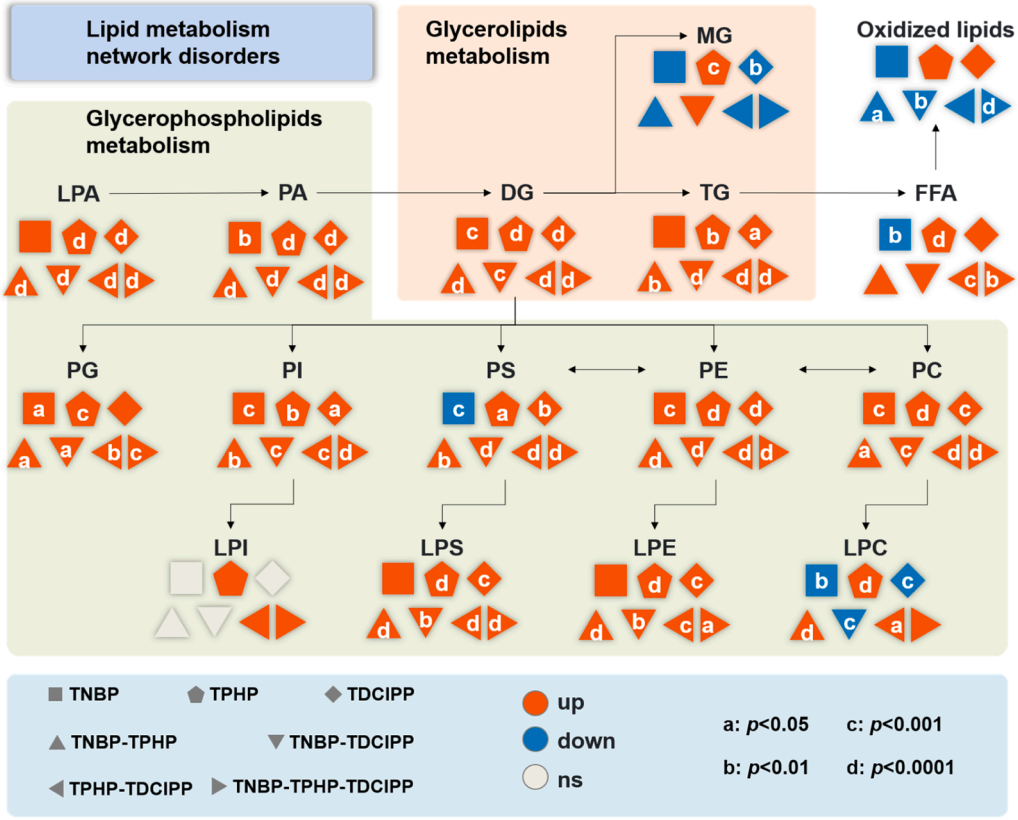


Fig. 7. Pathway-level reconstruction of lipid metabolic perturbations in HaCaT cells following OPE exposure. Differential regulation across glycerolipid (GL) and glycerophospholipid (GP) networks reveals compound-specific lipid remodeling patterns.

4. Conclusion

This study demonstrates that OPE mixture toxicity varies with mixture composition and effect level. The three OPEs also contributed differently to the observed interaction outcomes and exhibited distinct lipid metabolic response patterns. These experimentally supported findings indicate that mixture behavior cannot be fully characterized by single-compound toxicity alone. More broadly, these results suggest that interaction dynamics and component-specific biological responses may provide useful complementary information for mixture risk assessment. Future studies incorporating more complex exposure scenarios and direct mechanistic validation will further clarify the relevance of these findings to real-world chemical mixtures.

Statement of significance

OPE mixtures exhibit composition-dependent and dynamically shifting interactions, with TPHP promoting synergistic toxicity and TNBP attenuating mixture effects. Lipid metabolic remodeling provides a mechanistic link between these distinct interactions and skin barrier dysfunction, supporting mechanism-informed risk assessment of OPE mixtures.

CRediT authorship contribution statement

Yanpeng Gao: Writing – review & editing, Data curation, Conceptualization. **Taicheng An:** Writing – review & editing, Supervision, Project administration, Funding acquisition. **Na Luo:** Writing – original draft, Methodology, Investigation, Formal analysis. **Guiying Li:** Writing – review & editing, Supervision.

Declaration of Competing Interest

The authors declare no competing financial interests or relevant personal relationships.

Acknowledgements

This work was financially supported by National Natural Science Foundation of China (42530702 and 42507569), GuangDong Basic and Applied Basic Research Foundation (2023A1515110370), Postdoctoral Fellowship Program of CPSF (GZC20230566), China Postdoctoral Science Foundation funded project (2023M740749).

Appendix A. Supporting information

Supplementary data associated with this article can be found in the online version at doi:10.1016/j.jhazmat.2026.143996.

Data availability

No data was used for the research described in the article.

References

[1] Domingo, J.L., Nadal, M., 2026. Mixture toxicity in human health: integrating one health, exposomics, and modern risk assessment strategies. Chem Res Toxicol. https://doi.org/10.1021/acs.chemrestox.5c00375.
[2] Zhang, J., Liu, J., Ding, J., Yu, H., Li, Z., et al., 2025. Tris(2-chloroethyl) phosphate leads to unbalanced circulating erythrocyte in mice by activating both medullary and extramedullary erythropoiesis. Environ Sci Technol 199–211. https://doi.org/10.1021/acs.est.4c09436.
[3] Zhao, B., Zheng, S., Yang, G., He, Z., Deng, J., et al., 2025. Rap1 and mTOR signaling pathways drive opposing immunotoxic effects of structurally similar aryl-OPFRs, TPHP and TOCP. Environ Int 195, 109215. https://doi.org/10.1016/j.envint.2024.109215.

[4] Wan, M., Simonin, E.M., Johnson, M.M., Zhang, X., Lin, X., et al., 2025. Exposomics: a review of methodologies, applications, and future directions in molecular medicine. EMBO Mol Med 17, 599–608-608. https://doi.org/10.1038/s44321-025-00191-w.

[5] Gao, P., 2021. The Exposome in the Era of One Health. Environ Sci & Technol 55, 2790–2799. https://doi.org/10.1021/acs.est.0c07033.

[6] Wang, F., Xiang, L., Sze-Yin Leung, K., Elsner, M., Zhang, Y., et al., 2024. Emerging contaminants: A One Health perspective. Innovation 5, 100612. https://doi.org/10.1016/j.xinn.2024.100612.

[7] Guan, M., Zong, L., Xu, X., Zhang, S., Cao, D., et al., 2026. Unraveling Antagonistic Interactions in Complex Mixtures of Benzotriazole UV Stabilizers: A High-Throughput NAMs Approach Pinpoints Key Contributors and Underlying Pathways. Environ Sci & Technol. https://doi.org/10.1021/acs.est.5c15702.

[8] Yang, L., Zeng, J., Gao, N., Zhu, L., Feng, J., 2024. Predicting the Metal Mixture Toxicity with a Toxicokinetic–Toxicodynamic Model Considering the Time-Dependent Adverse Outcome Pathways. Environ Sci & Technol 58, 3714–3725. https://doi.org/10.1021/acs.est.3c09857.

[9] Ooka, M., Zhao, J., Zhang, L., Huang, R., Sakamuru, S., et al., 2025. Profiling of Environmental Mixtures Containing Metals for Their Toxicity Pathways and Mechanism of Action. Environ Sci & Technol 59, 4778–4787. https://doi.org/10.1021/acs.est.4c07995.

[10] Martin, O., Scholze, M., Ermler, S., McPhie, J., Bopp, S.K., et al., 2021. Ten years of research on synergisms and antagonisms in chemical mixtures: A systematic review and quantitative reappraisal of mixture studies. Environ Int 146, 106206. https://doi.org/10.1016/j.envint.2020.106206.

[11] Zhang, Y., Liu, M., Peng, B., Jia, S., Koh, D., et al., 2020. Impact of mixture effects between emerging organic contaminants on cytotoxicity: A systems biological understanding of synergism between tris(1,3-dichloro-2-propyl)phosphate and triphenyl Phosphate. Environ Sci & Technol 54, 10722–10734. https://doi.org/10.1021/acs.est.0c02188.

[12] Ma, H., Li, Z., Wang, D., Wang, X., Li, S., et al., 2026. Nationwide Indoor-Outdoor Exchange and Health Risks of Organophosphate Esters in China. Environ Sci & Technol 60, 8628–8638. https://doi.org/10.1021/acs.est.5c15217.

[13] Gong, H., Zhang, S., Xia, Z., Cao, X., Wang, Y., et al., 2026. Synthetic Fiber Sanitary Napkins: Nonnegligible Exposure Source of Organophosphate Esters in Women. Environ Sci & Technol 60, 10663–10672. https://doi.org/10.1021/acs.est.6c01183.

[14] Zhao, Y., Fan, Y., Li, J., Liu, Y., Lv, Y., et al., 2024. Assessment of human exposure to traditional and novel organophosphate esters via multiple personal matrices. Environ Sci & Technol 58 3332-3341. https://doi.org/10.1021/acs.est.3c07282.

[15] Xie, Z., Wang, P., Wang, X., Castro-Jiménez, J., Kallenborn, R., et al., 2022. Organophosphate ester pollution in the oceans. Nat Rev Earth & Environ 3, 309–322. https://doi.org/10.1038/s43017-022-00277-w.

[16] Li, W., Liu, Y., Song, Q., Zeng, Q., Chen, J., et al., 2025. Human exposure to organophosphate esters (OPEs): A meta-analytic review of levels and distribution. J Hazard Mater 496, 139496. https://doi.org/10.1016/j.jhazmat.2025.139496.

[17] Tang, J., Ma, S., Hu, X., Lin, M., Li, G., et al., 2023. Handwipes as indicators to assess organophosphate flame retardants exposure and thyroid hormone effects in e-waste dismantlers. J Hazard Mater 443, 130248. https://doi.org/10.1016/j.jhazmat.2022.130248.

[18] Du, Z., Ruan, Y., Chen, J., Fang, J., Xiao, S., et al., 2024. Global Trends and Hotspots in Research on the Health Risks of Organophosphate Flame Retardants: A Bibliometric and Visual Analysis. Toxics 391.

[19] Liao, K., Zhao, Y., Qu, J., Yu, W., Hu, S., et al., 2023. Organophosphate esters concentrations in human serum and their associations with Sjögren syndrome. Environ Pollut 331, 121941. https://doi.org/10.1016/j.envpol.2023.121941.

[20] Yuan, S., Zhang, H., Wang, S., Jiang, X., Ma, M., et al., 2024. Do the same chlorinated organophosphorus flame retardants that cause cytotoxicity and DNA damage share the same pathway? Ecotoxicol Environ Saf 273, 116158. https://doi.org/10.1016/j.ecoenv.2024.116158.

[21] Shi, S., Feng, Q., Zhang, J., Wang, X., Zhao, L., et al., 2024. Global patterns of human exposure to flame retardants indoors. Sci Total Environ 912, 169393. https://doi.org/10.1016/j.scitotenv.2023.169393.

[22] Wang, Z., Geng, S., Zhang, J., Yang, H., Shi, S., et al., 2024. Methods for the characterisation of dermal uptake: Progress and perspectives for organophosphate esters. Environ Int 183, 108400. https://doi.org/10.1016/j.envint.2023.108400.

[23] Zhang, R., Li, N., Li, J., Zhao, C., Luo, Y., et al., 2022. Percutaneous absorption and exposure risk assessment of organophosphate esters in children's toys. J Hazard Mater 440, 129728. https://doi.org/10.1016/j.jhazmat.2022.129728.

[24] Wang, X., Zhao, X., Shi, D., Dong, Z., Zhang, X., et al., 2023. Integrating Physiologically Based Pharmacokinetic Modeling-Based Forward Dosimetry and in Vitro Bioassays to Improve the Risk Assessment of Organophosphate Esters on Human Health. Environ Sci & Technol 57, 1764–1775. https://doi.org/10.1021/acs.est.2c04576.

[25] Yang, Y., Hou, Y., Liao, Y., Huang, Z., Pan, J., et al., 2025. Percutaneous penetration of typical Organophosphate esters under catalysis by Carboxylesterase: Characteristics, mechanism and prediction model. Environ Int 198, 109419. https://doi.org/10.1016/j.envint.2025.109419.

[26] Hu, F., Li, M., Chen, Y., Xie, K., Chen, Z., et al., 2026. Advancing environmental toxicology with lipidomics: from toxicity evaluation to mechanistic understanding. Ecotoxicology 35, 84. https://doi.org/10.1007/s10646-026-03060-5.

[27] Kiezel-Tsugunova, M., Kendall, A.C., Nicolaou, A., 2018. Fatty acids and related lipid mediators in the regulation of cutaneous inflammation. Biochem Soc Trans 46, 119–129. https://doi.org/10.1042/BST20160469.

[28] Vinggaard, A.M., Bonefeld-Jørgensen, E.C., Jensen, T.K., Fernandez, M.F., Rosenmai, A.K., et al., 2021. Receptor-based in vitro activities to assess human exposure to chemical mixtures and related health impacts. Environ Int 146, 106191. https://doi.org/10.1016/j.envint.2020.106191.

[29] Nazir, A., Cedergreen, N., 2014. Quantifying Synergy: A Systematic Review of Mixture Toxicity Studies within Environmental Toxicology. PLoS ONE 9. https://doi.org/10.1371/journal.pone.0096580.

[30] Ianevski, A., Giri, A.K., Aittokallio, T., 2022. SynergyFinder 3.0: an interactive analysis and consensus interpretation of multi-drug synergies across multiple samples. Nucleic Acids Res 50, W739–W743. https://doi.org/10.1093/nar/gkac382.

[31] Bajard, L., Vespalcová, H., Negi, C.K., Kohoutek, J., Bláha, L., et al., 2023. Anti-androgenic activity of novel flame retardants in mixtures: Newly identified contribution from tris(2,3-dibromopropyl) isocyanurate (TDBP-TAZTO). Chemosphere 341, 140004. https://doi.org/10.1016/j.chemosphere.2023.140004.

[32] Zhou, Y., Liao, H., Yin, S., Wang, P., Ye, X., et al., 2023. Aryl-, halogenated- and alkyl- organophosphate esters induced oxidative stress, endoplasmic reticulum stress and NLRP3 inflammasome activation in HepG2 cells. Environ Pollut 316, 120559. https://doi.org/10.1016/j.envpol.2022.120559.

[33] He, W., Ding, J., Gao, N., Zhu, L., Zhu, L., et al., 2024. Elucidating the toxicity mechanisms of organophosphate esters by adverse outcome pathway network. Arch Toxicol 98, 233–250. https://doi.org/10.1007/s00204-023-03624-y.

[34] Cui, D., Zhong, H., Ma, Z., Cheng, Y., Liu, C., et al., 2026. Dermal exposure to heavy metals contaminated soil from e-waste sites: Linking bioaccessibility to cellular uptake, cytotoxicity, and transport mechanisms in skin cells. J Hazard Mater 503, 141178. https://doi.org/10.1016/j.jhazmat.2026.141178.

[35] Chen, Q., Yi, S., Yang, L., Zhu, L., 2024. Penetration pathways, influencing factors and predictive models for dermal absorption of exobiotic molecules: A critical review. Sci Total Environ 927, 172390. https://doi.org/10.1016/j.scitotenv.2024.172390.

[36] Chen, Q., Yi, S., Ye, Q., Zhu, Y., Zhong, W., et al., 2022. Insights into the Dermal Absorption, Deposition, and Elimination of Poly- and Perfluoroalkyl Substances in Rats: The Importance of Skin Exposure. Environ Sci & Technol 56, 16975–16984. https://doi.org/10.1021/acs.est.2c03181.

[37] Guo, P., Chen, F., Zhao, M., 2026. Ferroptosis as a Pathogenic Mechanism and Therapeutic Target in Autoimmune and Inflammatory Skin Diseases. Clin Rev Allergy & Immunol 69, 34. https://doi.org/10.1007/s12016-025-09125-3.

[38] Menéndez-Pedriza, A., Jaumot, J., Bedia, C., 2022. Lipidomic analysis of single and combined effects of polyethylene microplastics and polychlorinated biphenyls on human hepatoma cells. J Hazard Mater 421, 126777. https://doi.org/10.1016/j.jhazmat.2021.126777.

[39] Negi, C.K., Gadara, D., Kohoutek, J., Bajard, L., Spáčil, Z., et al., 2023. Replacement Flame-Retardant 2-Ethylhexyldiphenyl Phosphate (EHDPP) Disrupts Hepatic Lipidome: Evidence from Human 3D Hepatospheroid Cell Culture. Environ Sci & Technol 57, 2006–2018. https://doi.org/10.1021/acs.est.2c03998.

[40] van der Veen, J.N., Kennelly, J.P., Wan, S., Vance, J.E., Vance, D.E., et al., 2017. The critical role of phosphatidylcholine and phosphatidylethanolamine metabolism in health and disease. Biochim Et Biophys Acta (BBA) - Biomembr 1859, 1558–1572. https://doi.org/10.1016/j.bbamem.2017.04.006.

[41] Dai, Q., Xie, P., Tan, H., Zhang, J., Wang, F., et al., 2024. Metabolomics and Lipidomics with Mass Spectrometry Imaging Reveal Mechanistic Insights into Dibutyl Phthalate-Promoted Proliferation of Breast Cancer Cell Spheroids. Environ Sci & Technol Lett 11, 208–215. https://doi.org/10.1021/acs.estlett.4c00048.

[42] van Meer, G., 2005. Cellular lipidomics. EMBO J 24, 3159–3165. https://doi.org/10.1038/sj.emboj.7600798.

[43] Klose, C., Surma, M.A., Simons, K., 2013. Organellar lipidomics—background and perspectives. Curr Opin Cell Biol 25, 406–413. https://doi.org/10.1016/j.ceb.2013.03.005.

[44] Seu, K.J., Cambrea Lr Fau - Everly, R.M., Everly Rm Fau - Hovis, J.S., Hovis, J.S., 2006. Influence of lipid chemistry on membrane fluidity: tail and headgroup interactions. Biophys J 91, 3727–3735.

[45] Wu, J., Zhou, J.-H., Liu, D.-F., Wu, J., He, R.-L., et al., 2023. Phthalates Promote Dissemination of Antibiotic Resistance Genes: An Overlooked Environmental Risk. Environ Sci & Technol 57, 6876–6887. https://doi.org/10.1021/acs.est.2c09491.

[46] Chen, J., Xie, P., Wu, P., Lin, Z., He, Y., et al., 2023. Spatial Metabolomics and Lipidomics Reveal the Mechanisms of the Enhanced Growth of Breast Cancer Cell Spheroids Exposed to Triclosan. Environ Sci & Technol 57, 10542–10553. https://doi.org/10.1021/acs.est.3c01746.

[47] Kim, K.-H., Yoo, B.C., 2026. Decoding Membrane Lipids: Analytical Barriers and Technological Advances in Modern Lipidomics. Int J Mol Sci 1472.

[48] Pyambri, M., Lacorte, S., Jaumot, J., Bedia, C., 2023. Effects of Indoor Dust Exposure on Lung Cells: Association of Chemical Composition with Phenotypic and Lipid Changes in a 3D Lung Cancer Cell Model. Environ Sci & Technol 57, 20532–20541. https://doi.org/10.1021/acs.est.3c07573.

[49] Jin, Y., Shi, H., Zhao, Y., Dai, J., Zhang, K., 2024. Organophosphate ester cresyl diphenyl phosphate disrupts lipid homeostasis in zebrafish embryos. Environ Pollut 342, 123149. https://doi.org/10.1016/j.envpol.2023.123149.

[50] Dyall, S.C., Balas, L., Bazan, N.G., Brenna, J.T., Chiang, N., et al., 2022. Polyunsaturated fatty acids and fatty acid-derived lipid mediators: Recent advances in the understanding of their biosynthesis, structures, and functions. Progress Lipid Res 86, 101165. https://doi.org/10.1016/j.plipres.2022.101165.

[51] Lee, Y.J., Choi, H.-I., Hwang, J.-h, Park, M., Choi, M., et al., 2026. Phosphatidylserine-Rich circulating extracellular vesicles activate TAM receptor signaling to promote skin wound repair. Biochem Pharmacol 249, 117941. https://doi.org/10.1016/j.bcp.2026.117941.

[52] Lee, S.-H., Yang, J.-H., Park, Y.-K., Han, J.-J., Chung, G.-H., et al., 2013. Protective effect and mechanism of phosphatidylserine in UVB-induced human dermal

fibroblasts. Eur J Lipid Sci Technol 115, 783–790. https://doi.org/10.1002/ejlt.201200086.

[53] Doktorova, M., Symons, J.L., Zhang, X., Wang, H.-Y., Schlegel, J., et al., 2025. Cell membranes sustain phospholipid imbalance via cholesterol asymmetry. e2524 Cell 188, 2586–2602. https://doi.org/10.1016/j.cell.2025.02.034.

[54] Li, Y.-P., Liu, C., Mustieles, V., Zhang, Y., Messerlian, C., et al., 2025. Organophosphate esters, sperm mitochondrial DNA copy number, and semen quality: a longitudinal study with repeated measurements. Environ Sci Technol 59, 3388–3400. https://doi.org/10.1021/acs.est.4c09573.

[55] Gao, P., 2024. Chasing "Emerging" contaminants: an endless journey toward environmental health. Environ Sci Technol 58, 1790–1792. https://doi.org/10.1021/acs.est.3c10630.

[56] Qadeer, A., Mubeen, S., Liu, M., Bekele, T.G., Ohoro, C.R., et al., 2024. Global environmental and toxicological impacts of polybrominated diphenyl ethers versus organophosphate esters: a comparative analysis and regrettable substitution dilemma. J Hazard Mater 466, 133543. https://doi.org/10.1016/j.jhazmat.2024.133543.